JOC The Journal of Organic Chemistry

Article

pubs.acs.org/joc

Synthesis and Properties of Axially Symmetrical Rigid Visible Light-Harvesting Systems Containing [60]Fullerene and Perylenebisimide

San-E Zhu,[†] Kai-Qing Liu,[†] Xue-Fei Wang,*[,‡] An-Dong Xia,[§] and Guan-Wu Wang*[,†]

[†]CAS Key Laboratory of Soft Matter Chemistry, Hefei National Laboratory for Physical Sciences at Microscale and Department of Chemistry, University of Science and Technology of China, Hefei, Anhui 230026, P. R. China

[‡]School of Chemistry and Chemical Engineering, University of Chinese Academy of Sciences, Beijing 100049, China

[§]The State Key Laboratory of Molecular Reaction Dynamics and Beijing National Laboratory for Molecular Sciences (BNLMS), Institute of Chemistry, Chinese Academy of Sciences, Beijing 100190, P. R. China

Supporting Information

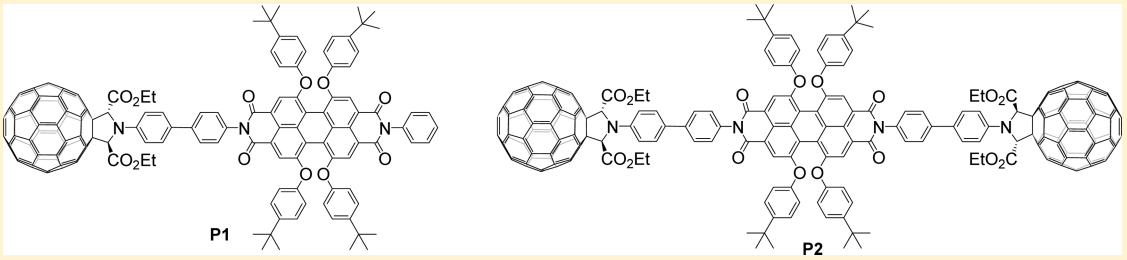

ABSTRACT: Two visible light-harvesting perylenebisimide (PDI)-[60]fullerene (C_{60}) systems, dyad **P1** with one C_{60} unit and triad **P2** with two C_{60} units, have been synthesized. Both systems are axially symmetrical with a rigid biphenyl linker, ensuring a relatively fixed spatial distance between the donor and acceptor, preventing through-space interaction, and enhancing energy transfer. Steady-state and transient spectroscopy, electrochemistry, as well as theoretical calculations have been used to investigate the electrochemical and photophysical properties of the two systems. Steady-state and time-resolved spectroscopy demonstrate that the excited state is featured by an efficient intramolecular energy transfer from PDI to C_{60}. Then, the high efficient intrinsic intersystem crossing of C_{60} eventually leads to the production of the triplet C_{60}. The extensive visible light absorption of PDI in the range of 400−650 nm and the final localization of the excited energy at the triplet C_{60} make these compounds ideal singlet oxygen inducers. Further investigation shows that the photooxidation capability for both compounds is significantly enhanced with respect to either PDI or C_{60} and even better than that of the commonly used triplet photosensitizer methylene blue (MB). The double C_{60} moieties in **P2** display a better result, and the photooxidation efficiency of **P2** increases 1.3- and 1.4-fold compared to that of **P1** and MB, respectively. The combination of a light-harvesting unit with an intersystem crossing unit results in a highly efficient photooxidation system, which opens up a new way to triplet photosensitizer design.

INTRODUCTION

In recent decades, fullerenes and their derivatives have gained increasing attention because of their special photophysical features such as low excited state, low reduction potential,[1] good thermal stability,[2] as well as low cost and environmental friendliness.[3] In particular, because of the conjugated π-network covering the entire molecular surface,[4] fullerenes exhibit important photophysical characteristics, i.e., high intrinsic intersystem crossing (ISC) efficiency,[1,5] which results in a high triplet state yield (~1). The triplet fullerenes, whose long lifetimes benefit energy storage, have been verified as good sensitizers of singlet oxygen used in photodynamic therapy.[6,7] However, the weak absorption in the visible range imposes a significant limitation on the application of fullerenes. In natural photosynthesis, the photon energy is utilized efficiently through energy or electron transfer from the light-harvesting antenna pigment to the reaction center and has proven to be of high quantum yield. Inspired by the natural system, molecules exhibiting high extinction coefficients in the visible region have been connected to fullerenes as light-harvesting antennas.[3,8−16]

Similarly, the energy can be utilized by the artificial systems comprising an antenna moiety and a fullerene motif through two pathways, i.e., charge separation and energy transfer. In the case of charge separation, the dye moieties such as porphyrin derivatives[17,18] and oligothienyls[19,20] should have the first reduction potential lower than that of fullerenes besides their good spectral matching, whereas in the case of energy transfer, both moieties should possess similar reduction potentials. To finish the energy transfer from dyes to fullerenes, the excited state level of the former, such as subphthalocyanines,[21] should be closer to but somewhat higher than that of the latter. Both mechanisms have been applied in different fields, for example, charge separation in photovoltaic systems[22,23] and energy transfer in photosensitized reactions.[3,13,14,16,24]

Received: August 19, 2016
Published: November 9, 2016

DOI: 10.1021/acs.joc.6b02042
J. Org. Chem. 2016, 81, 12223−12231

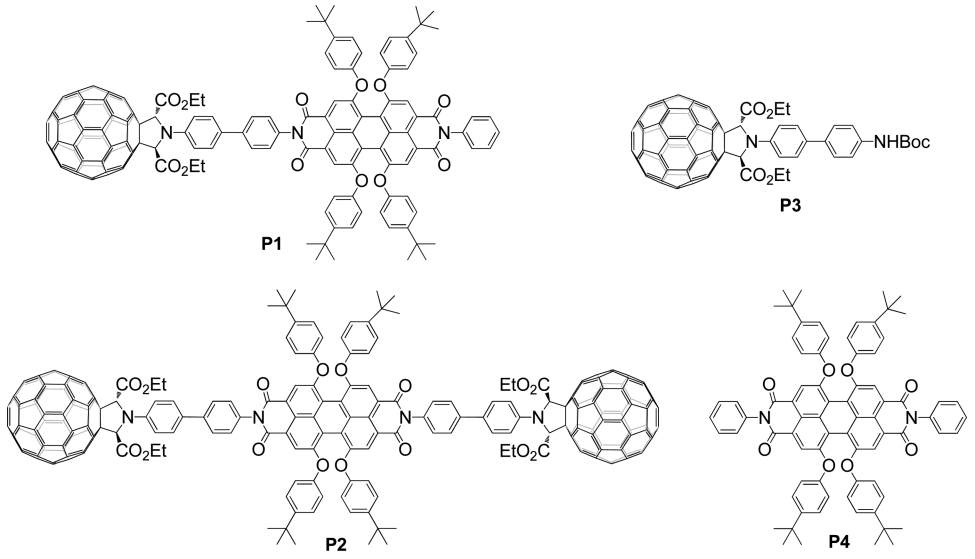

Figure 1. Molecules synthesized and studied in the present work.

Scheme 1. Synthetic Procedures for P1−P4[a]

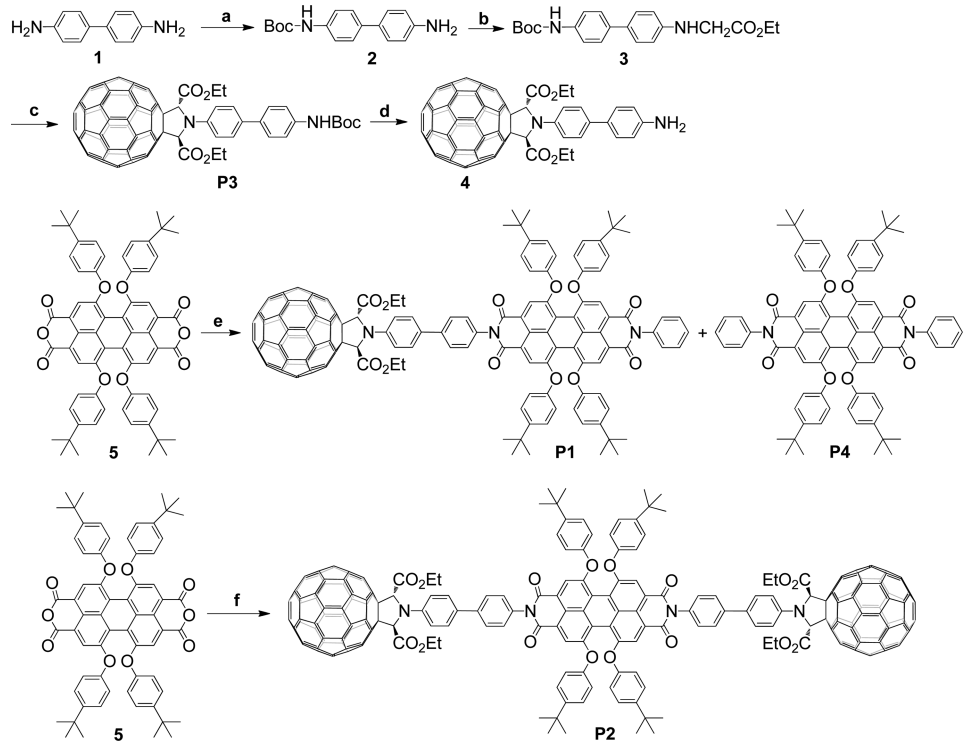

[a](a) Boc_2O, 1,4-dioxone, Ar, rt, 24 h, 85%; (b) $BrCH_2CO_2Et$, K_2CO_3, DMF, Ar, rt, 12 h, 68%; (c) C_{60}, $HCOCO_2Et$, ODCB, Ar, 150 °C, 4 h, 35%; (d) TFA, $CHCl_3$, Ar, rt, 2 h, 95%; (e) **4**, imidazole, $CHCl_3$, Ar, 80 °C, 3 d; then aniline, Ar, 80 °C, 24 h, **P1** (36%) + **P4** (38%); (f) **4**, imidazole, $CHCl_3$, Ar, 90 °C, 5 d, 44%.

Perylenebisimides (PDIs) are well-known chromophores combining high quantum yield of photoluminescence with excellent photochemical and thermal stability and have been successfully used in field-effect transistors,[25] electroluminescent devices,[26] and solar energy conversion areas.[27,28] Moreover, PDIs are characteristic of low reduction potential close to that of [60]fullerene (C_{60}),[27,29] which makes them ideal for fundamental studies to address photoinduced energy transfer in new donor−acceptor systems. In addition, PDI derivatives and related compounds are known to exhibit strong two-photon absorption,[30,31] which extends the excitation light to the NIR region and are of interest for biological applications.

In this study, we designed and synthesized two axially symmetrical rigid visible light-harvesting systems, PDI-[60]-fullerene dyad **P1** (PDI-C_{60}) and triad **P2** (C_{60}-PDI-C_{60}) (Figure 1), investigated their photophysical properties through steady-state and transient spectra, electrochemistry, and theoretical calculations, and further explored their photo-oxidation capability. In previous studies, flexible linkages between the PDI and fullerene subunits have been used in

DOI: 10.1021/acs.joc.6b02042
J. Org. Chem. 2016, 81, 12223−12231

most cases, leading to complex dynamic processes owing to the varying distances between PDI and C_{60} units in different folded and extended conformers.[32−34] It has been reported that rigid spacers between porphyrin and C_{60} could prevent through-space interaction and enhance electron transfer.[35,36] Inspired by this, a rigid bridge (biphenyl) was employed between PDI and C_{60} in the present work to ensure a relatively fixed spatial distance between the donor and acceptor. For the photophysical processes to be simplified further, the PDI and C_{60} were connected through the nitrogen atoms of the fulleropyrrolidine and perylenebisimide moieties with a biphenyl linker, where the axially symmetrical structure would lead to a more efficient energy and/or electron transfer between PDI and C_{60}.[36] Previously, to increase photon-harvesting capability, more PDIs have been attached to one C_{60};[29] however, this protocol inevitably leads to a slightly lower energy-transfer efficiency than that with one PDI moiety due to the long triplet-state lifetime of the C_{60} moiety (40 μs)[7] during which period PDI would not transfer energy to C_{60} but rather would undergo fluorescence emission within lifetime at the nanosecond level. Taking this into consideration, we deliberately attached the second C_{60} moiety to PDI, providing a triad C_{60}-PDI-C_{60} that possessed two pathways to receive the excited energy of PDI.

RESULTS AND DISCUSSION

Synthesis. Besides target molecules **P1** and **P2**, **P3** and **P4** were also synthesized as reference compounds (Scheme 1). The strategy employed for the preparation of **P1**, **P2**, and **P4** is based upon the efficient amidation reaction of 3,4,9,10-perylenetetracarboxylic dianhydride (PDA). The initial effort was focused on the synthesis of fulleropyrrolidine **4** with amino as the terminal group, which was produced by deprotection of **P3**. Compound **P3** was prepared by the 1,3-dipolar cycloaddition of the azomethine ylide generated in situ from the condensation of amino acid ester **3** with glyoxylic acid ethyl ester to C_{60}, as outlined in Scheme 1. First, Boc_2O was selected to protect one of the amino groups of benzidine **1** in 1,4-dioxane at room temperature for 24 h under argon atmosphere, giving **2**[37] in 85% yield. Then, **2** was reacted with ethyl bromoacetate in DMF with K_2CO_3 as a base at room temperature for 12 h to provide **3** in 68% yield. After reaction of **3** with glyoxylic acid ethyl ester and C_{60} in *o*-dichlorobenzene (ODCB) at 150 °C for 4 h, Boc-protected fulleropyrrolidine **P3** was isolated in 35% yield. The Boc-group could be easily removed by TFA in $CHCl_3$ at room temperature within 2 h to afford **4** in 95% yield. PDA and its monoanhydride derivatives have strong adsorption on a silica gel column when separated by column chromatography. For the adsorption to be avoided, **P1** was synthesized by cross-condensation of aniline, fulleropyrrolidine **4**, and PDA **5**. The mixture was stirred in $CHCl_3$ with imidazole as the base afforded **P1** as the target product in 36% yield along with **P4** as a reference compound in 38% yield. **P2** was similarly synthesized in 44% yield by the amidation reaction of **5** with 2.5 equiv of fulleropyrrolidine **4** at 90 °C for 5 days.

The introduction of the *tert*-butylphenoxy groups at the perylene bay region greatly improved the solubility of compounds **P1** and **P2**, thus allowing their full spectroscopic and electrochemical characterization. The IR spectra of **P1** and **P2** showed characteristic absorption of C_{60} at approximately 530, 580, and 1175 cm^{-1}, respectively, and the characteristic absorption pattern of the perylene skeleton with bands at approximately 1500 and 1590 cm^{-1}. The ^1H NMR spectra of **P1** and **P2** in $CDCl_3$ also gave all expected signals, such as those corresponding to the perylene skeleton protons (two singlets at 8.25 and 8.29 ppm for **P1** and a singlet at 8.29 ppm for **P2**) and methine protons of the pyrrolidine ring (a singlet at 6.57 ppm for both **P1** and **P2**). In the ^{13}C NMR spectra of **P1** and **P2**, no more than 27 peaks were seen in the 135−154 ppm range for the sp^2 carbons of the C_{60} cage, and one peak at ~71 ppm for the sp^3 carbons of the C_{60} skeleton, which is consistent with the molecular symmetry of C_2 for **P1** and C_{2v} for **P2**. The structures of **P1** and **P2** were also characterized by MALDI-TOF mass spectroscopy with molecular peaks at m/z 2116.5893 and 3098.6865, respectively. Full characterizations of the reference compounds **P3** and **P4** were similarly achieved due to their good solubilities.

Steady-State Absorption and Emission. The UV−vis absorption spectra of **P1** and **P2** in toluene are shown in Figure 2a. For comparison, the spectra of the reference compounds **P3** and **P4** are also included. Compounds **P1** and **P2** revealed strong absorptions at 535 and 575 nm and relatively weak absorption around 448 nm that came from the PDI moiety, together with strong absorption in the UV region from the C_{60} moiety. The UV−vis spectra of **P1** and **P2** were essentially the superimposition of reference compounds **P3** and **P4** in a 1:1 and 2:1 ratio, respectively, implying that the electronic interactions between C_{60} and PDI moieties in both **P1** and **P2** were negligible at the ground state. The UV−vis absorption spectra of **P1**−**P4** in the solid state were also investigated and are shown in Figure S1a. Compared with the spectra in solution at low concentration, broader absorption spectra were observed for all four compounds.

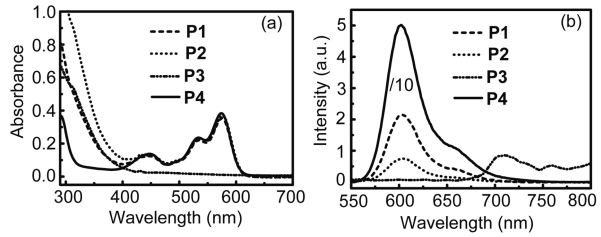

Figure 2. (a) UV−vis absorption spectra of **P1** (dashed line), **P2** (dotted line), **P3** (dashed-dotted-dotted line), and **P4** (solid line) in toluene (c = 1.0 × 10^{-5} mol L^{-1}). (b) Fluorescence of **P1**−**P4** in toluene (excited at 450 nm, c = 1.0 × 10^{-6} mol L^{-1} for **P1**, **P2**, and **P4** and c = 1.0 × 10^{-5} mol L^{-1} for **P3**). For clarity, the emission intensity of **P4** was divided by 10.

Chromophore PDI has been investigated widely for its high emission efficiency.[38] Herein, the fluorescence spectra of the four compounds in toluene have been measured and are shown in Figure 2b. From the results, it can be found that **P1**, **P2**, and **P4** exhibited similar spectral profiles with characteristic features of the PDI unit. However, the luminescence of **P1** at 603 nm is largely quenched (96%), suggesting that the excited singlet state of the PDI moiety (^{1}PDI*) was quenched by the C_{60} moiety via photoinduced energy transfer[33,34,39,40] and/or electron transfer.[27,32,41−43] The luminescence quenching of approximately 98% for **P2** at 603 nm indicated a more efficient quenching of the perylenebisimide fluorescence in the system containing two fullerene units. It is interesting to note that a more efficient fluorescence quenching (≥96%) for **P1** and **P2** was observed compared to that (~88.4%) for a similar

DOI: 10.1021/acs.joc.6b02042
J. Org. Chem. 2016, 81, 12223−12231

compound with a flexible linker between C_{60} and PDI.[33] When excited at 450 nm, **P3** exhibited a weak emission at 709 nm arising for the fullerene chromophore. However, this emission band was not observed in both **P1** and **P2** due to the weak visible light absorption and low fluorescence yield of C_{60}[44] as well as the overlapping by the fluorescence emission of PDI. The fluorescence spectra of **P1**, **P2**, and **P4** in tetrahydrofuran (THF), which has a very different polarity compared with toluene, were also measured (see Figure S2), and no apparent change was observed in the emission peak positions. The low solvent effect indicated the formation of a neutral excited state because charge-separated states are normally characterized by significant emissive response to solvent polarity.[45,46] Thus, the emission quenching observed here should be ascribed to the intramolecular energy transfer from PDI to C_{60}. It can be predicted that the energy-transfer process would eventually lead to the formation of the triplet C_{60} due to its high ISC efficiency,[1,5] which resulted in high triplet state yield (~1). The fluorescence spectra of the four compounds in the solid state were also measured, and are shown in Figure S1b. Compared with the spectra in solution at low concentration, the emission peak of **P4** was shifted to 680 nm, whereas no emission bands were observed for **P1**−**P3** in the solid state under the same measured conditions.

Electrochemical Studies. C_{60}, as one of the best electron acceptors, has been widely investigated in the photoelectron transfer system,[47−50] where C_{60} is usually attached to one or more light antennas and behaves as the electron-acceptor from the antenna. In this study, more attention was paid to the triplet formation of C_{60}. We believed that the emission quenching observed above arose from an energy transfer from antenna to C_{60} rather than from charge separation caused by electron transfer. To obtain information on the reduction potential of PDI and C_{60}, which was the premise of electron transfer in the dyad and triad, cyclic voltammograms of **P1**−**P4** were measured (Figure 3), and the redox potentials are collected

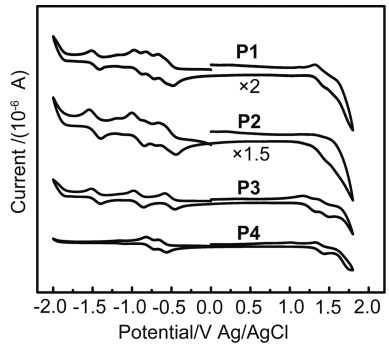

Figure 3. Cyclic voltammograms of dyad **P1** and triad **P2** along with references **P3** and **P4**.

in Table 1. By comparison with the data of reference compounds **P3** and **P4**, the second redox potentials of **P1** and **P2** could be attributed to the second reduction potential of the PDI moiety, and the third and the fourth reduction redox waves arose from the second and third reduction processes of the fullerene moiety. In agreement with the literature,[29,42] a broader first reduction wave was observed for both **P1** and **P2**, indicating overlap of the first reduction peak of C_{60} and PDI moieties. The close first reduction potential suggested a lower probability of the electron-transfer process between C_{60} and PDI. Therefore, the fluorescence quenching of the PDI moiety in **P1** and **P2** should be attributed to energy transfer.

Time-Resolved Fluorescence Spectroscopy. For deeper insight into the photophysical properties of the excited state to be obtained, the fluorescence decays of these compounds were recorded using time-correlated single photon counting (TCSPC). The fluorescence decay at 603 nm due to PDI was monoexponential (τ = 5.9 ns) for **P4** in toluene, and the decay curve is shown in Figure S3a. The decay curves of **P1** and **P2** at 603 nm attributed to the PDI moiety in toluene are shown in Figure 4. For both traces, two exponential processes were required to obtain the best fitting: the shorter one (τ = 0.2 ns) corresponded to the energy transfer process from PDI to C_{60}, and the longer one (τ = 5.9 ns) was assigned to the fluorescence lifetime of PDI.[32] The high percentage of the short-lived fluorescent component in both **P1** and **P2** indicated that the introduction of C_{60} resulted in effective excitation energy quenching of the PDI unit. Consistent with the steady-state emission results, a higher percentage (95%) of the short-lived fluorescent component in **P2** relative to that of **P1** (83%) was observed. For comparison, the fluorescence decays of **P1**, **P2**, and **P4** in the solid state were also measured. The decay curve of **P4** in the solid state is shown in Figure S3b, and the fluorescence lifetime recorded at 680 nm was 3.2 ns, which was slightly shorter than that (5.9 ns) in toluene. Unfortunately, we failed to record the emission dynamics of both **P1** and **P2** due to the strong quenching of the PDI chromophore by C_{60}.

TD-DFT Calculations. TD-DFT calculations were carried out at the CAM-B3LYP/3-21G level to figure out the excited-state charge distribution. Herein, the excited-state properties were characterized with the three-dimensional cube representation of the charge difference density (CDD),[51,52] which illustrated the distribution of net change in electron density as a result of electronic transition and the orientation of the possible intermolecular charge transfer (ICT) process. Figure 5 shows the CDD of Franck−Condon state and the lowest excited state of **P1**, displaying the intramolecular charge transfer orientation just upon excitation and that after suffering possible vibration relaxation, energy, or electron transfer processes. From the calculated results, it was found that although the holes (green) and electrons (red) could be distinguished from each other, both of them distributed all at the PDI unit for the initial state and then all at the C_{60} unit for the final state. The failed observation of a significant charge separation between PDI and C_{60} at excited states in CDD provided further evidence that the observed emission quenching should be ascribed to energy transfer from PDI to C_{60} rather than electron transfer. A similar CDD feature was obtained in **P2** (see Figure S4). Furthermore, C_{60} has also been known as a material with a high triplet yield (~1) through intersystem crossing.[1,5] As a result, it is logically accepted that the light energy harvested by the PDI moiety would be stored in these systems in the form of the triplet C_{60}, which has been shown to be an effective singlet oxygen inducer.

Nanosecond Time-Resolved Transient Absorption Spectroscopy. Nanosecond time-resolved transient absorption spectroscopy was utilized to characterize features of the triplet state of these systems. The transient absorption spectra of **P1** and **P2** in toluene are shown in Figure 6. As expected, a typical transient absorption band between 600 and 800 nm with a well-defined maximum around 700 nm for the triplet C_{60} was observed.[1,34] In the control experiment, the spectra of both **P3** and **P4** were also recorded, where **P3** showed a C_{60} moiety

DOI: 10.1021/acs.joc.6b02042
J. Org. Chem. 2016, 81, 12223−12231

Table 1. Redox Potentials (CV) of P1−P4[a]

	$E_{1/2}$ (1st red.)	$E_{1/2}$ (2nd red.)	$E_{1/2}$ (3rd red.)	$E_{1/2}$ (4th red.)
P1	−0.58 (0.20)[b]	−0.77 (0.10)[c]	−0.92 (0.10)[d]	−1.46 (0.10)[d]
P2	−0.55 (0.20)[b]	−0.76 (0.13)[c]	−0.93 (0.16)[d]	−1.47 (0.14)[d]
P3	−0.52 (0.13)	−0.92 (0.13)	−1.46 (0.12)	
P4	−0.61 (0.11)	−0.77 (0.10)		

[a]All potentials reported as $E_{1/2}$ (= $(E^a_p + E^c_p)/2$) in V vs SCE; the values in parentheses are ($E^a_p - E^c_p$) for the redox couples with platinum electrode as the working electrode, platinum wire electrode as counter electrode, and calomel electrode as standard electrode. **P1−P4** are in ODCB using tetrabutylammonium perchlorate as supporting electrolyte. Scan rate = 100 mVs^{-1}. [b]Reduction potential associated with both C_{60} and perylenebisimide. [c]Reduction potential associated with perylenebisimide. [d]Reduction potential associated with C_{60}.

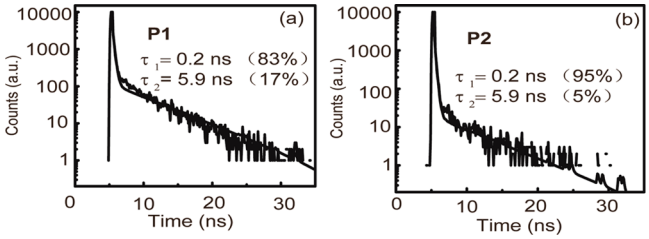

Figure 4. Fluorescence decay traces obtained with TCSPC of **P1** and **P2** in toluene and the corresponding dual-exponential function fitting results excited at 450 nm and recorded at 603 nm.

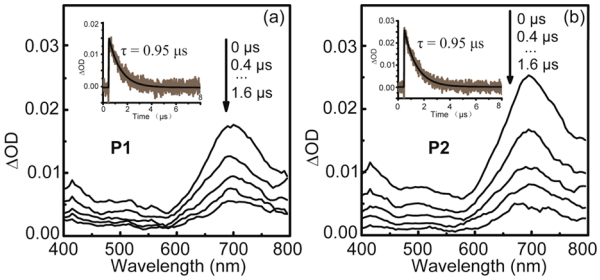

Figure 6. Representative transient absorption spectra of (a) **P1** and (b) **P2** in deaerated toluene observed at a series of delay times after excitation (532 nm, 7 ns fwhm, 2 mJ/pulse) at room temperature. Arrows indicate the spectral trend with increasing time. Insets show the dynamic curves and transient absorption time profiles of **P1** and **P2** at 710 nm.

triplet profile (see Figure S5a) and **P4** did not give significant absorption during the measurement time scale. Taking the possible intermolecular energy transfer due to collision into consideration, the solution of a mixture of **P3** and **P4** with a ratio of 1:1 was measured under the same conditions (see Figure S5b). As expected, no significant enhancement was observed in the spectrum of the mixture compared with that of **P3**, indicating that the energy transfer from donor to acceptor took place only intramolecularly in the dyad and triad and not between the reference compounds **P3** and **P4** distributed in solution. The pronounced formation of the C_{60} triplet in both dyad and triad suggested a potential ability to induce singlet oxygen in solution.

Another striking feature of the data is that the ΔOD for **P2** was somewhat higher than that for **P1** at the same delay time. Notably, the initial absorbance of both compounds at 532 nm was made sure to be identical with a value of 0.18, and the measurement was carried out under identical conditions. This suggested that although both molecules harvested the same amount of photons, the yield of the triplet C_{60} moiety in **P2** was relatively higher than that in **P1**. According to the discussion above, once the PDI moiety was excited, its singlet state energy was going to transfer to C_{60} within 1 ns and subsequently generate the triplet C_{60} with a longer lifetime of ∼1 μs. For **P1** with one C_{60} unit, once the C_{60} unit reached its triplet state, within the triplet state lifetime, it was not able to accept more energy from the singlet PDI, which had been excited by the following photon. In this case, the singlet PDI would be deactivated via fluorescence or other radiationless deactivation. In comparison, **P2** had two C_{60} units, and the subsequent energy had a chance to be transferred to another C_{60} unit. In the case of the nanosecond time-resolved transient experiment, a nanosecond pulsed laser with pulse width of 7 ns, which was longer than the lifetime of the singlet PDI, and a laser output of 2 mJ/pulse made it possible to excite the PDI unit twice or even more times within a single pulse; thus, a relatively higher triplet C_{60} signal was observed in **P2**. Herein, we observed a signal enhancement in **P2** by a factor of 1.5 with respect to **P1** rather than the expected 2-fold proportional to the number of the C_{60} unit. This could be ascribed to the laser intensity, which was assumed to lead to a nonlinear effect on the yield of the triplet C_{60}.

Singlet Oxygen Production. For the ability of the dyad and triad as photosensitizers to be demonstrated, the photooxidation experiment was performed by using 1,5-dihydroxy naphthalene (DHN) as a chemical sensor, which

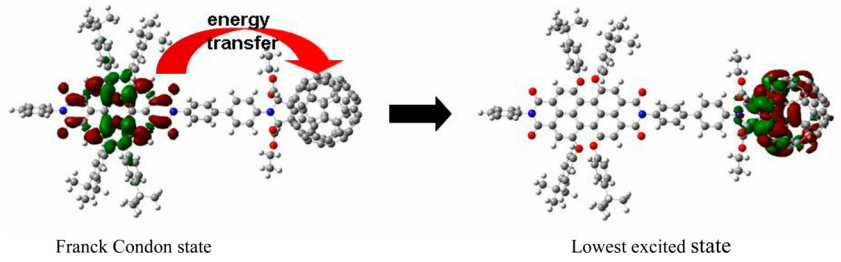

Figure 5. CDD of Franck−Condon state and the lowest excited state of **P1**. The negative density (green) corresponds to hole and the positive (red) to electron.

DOI: 10.1021/acs.joc.6b02042
J. Org. Chem. 2016, 81, 12223−12231

could be oxidized by $^1O_2$ to give an intermediate peroxide and then produced juglone.[53] The pathway for the reaction of DHN with $^1O_2$ leading to juglone is given in Scheme 2.[53,54]

Scheme 2. Reaction Mechanism for the Photooxidation of DHN with a Singlet Oxygen Photosensitizer

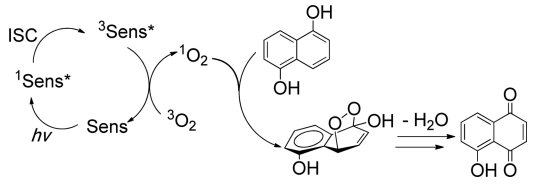

The spectral response of DHN using **P2** as the sensitizer upon photoirradiation by a xenon lamp is presented in Figure 7a, where the absorption of DHN at 301 nm decreased and the

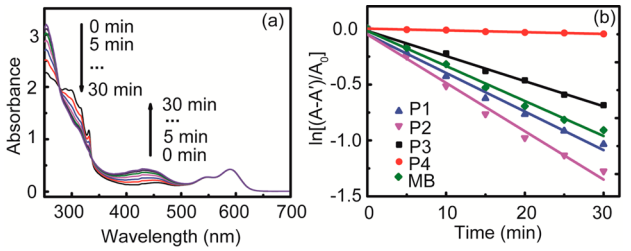

Figure 7. (a) Absorption spectral evolution for the photooxidation of DHN using **P2** as sensitizer. (b) Plots of $\ln[(A - A')/A_0]$ vs irradiation time (t) for the photooxidation of DHN using different sensitizers (collected at 301 nm). c[sensitizers] = 1.0×10^{-5} mol L^{-1}, c[DHN] = 1.0×10^{-4} mol L^{-1}. In CH_2Cl_2/MeOH (9:1, v/v). A, A', and A_0 were the absorbances at 301 nm where A was the absorption of DHN and sensitizer, A' was the absorption of sensitizer, A_0 was the initial absorption of DHN.

absorption of juglone at 427 nm increased with time, demonstrating the generation of singlet oxygen in solution. The photooxidation of DHN with **P1**, the reference compounds **P3** and **P4**, along with the typical organic triplet sensitizer methylene blue (MB) was also studied (Figure S6). **P2** exhibited the most significant UV−vis absorption change in the investigated samples. A similar spectral response of DHN with **P1** as the sensitizer was obtained, whereas the change was smaller than with **P2**. The photostabilities of **P1** and **P2** were also studied by exposure to light for 1 h, and no bleaching was observed (see Figure S7), demonstrating that the spectral alteration observed above was caused by the photooxidation of DHN instead of photobleaching. The kinetics of photooxidation of the sensitizers could be quantified by following the decrease rate of the absorbance at 301 nm.[55] The observed rate constants (k_{obs}) of the sensitizers were calculated by using a linear least-squares fitting of the plot of $\ln[(A - A')/A_0]$ relative to the irradiation time (Figure 7b).

With the typical organic triplet sensitizer methylene blue (MB) [Φ_Δ(std) = 0.57 in CH_2Cl_2] as a reference,[16] the singlet oxygen quantum yield (Φ_Δ) of **P1**−**P4** could be obtained by using eq 1.[55]

$$\Phi_\Delta = \Phi_\Delta(\text{std})\frac{k_{obs}(x)\cdot I(\text{std})}{k_{obs}(\text{std})\cdot I(x)} \quad (1)$$

where k_{obs}(x) and k_{obs}(std) were the absolute values of the slopes of $\ln[(A - A')/A_0]$ relative to irradiation time for the photooxidation of DHN by **P1**−**P4** and MB, respectively. I(x) and I(std) were the total light intensities absorbed by **P1**−**P4** and MB, respectively. The data are listed in Table 2.

Table 2. Photophysical Parameters of P1−P4 and the Reference MB[a]

	λ_{abs}[a]	λ_{em}[a]	k_{obs}[b]/min^{-1}	v_i[c]	Φ_Δ[d]
P1	311, 456, 544, 586	614, 671, 705	34.5	34.5	0.70
P2	311, 456, 544, 586	614, 671, 705	43.3	43.3	0.84
P3	311	705	22.5	22.5	0.86[e]
P4	456, 544, 586	614, 671	1.57	1.57	0.03
MB	292, 602, 655	*f*	31.3	31.3	0.57[g]

[a]In $CHCl_3$; $c = 1.0 \times 10^{-6}$ mol L^{-1}. [b]The rate constant k_{obs} was calculated by the rule: $\ln[(A - A')/A_0] = -k_{obs}t$; in 10^{-3} min^{-1}. A, A', and A_0 were the absorbances at 301 nm. [c]Initial consumption rate of DHN, $v_i = k_{obs}$[DHN]; in 10^{-7} M min^{-1}. [d]Quantum yield of singlet oxygen ($^1O_2$) with MB as standard (Φ_Δ = 0.57 in CH_2Cl_2). [e]The Φ_Δ of C_{60} was between 0.76 and 0.96 according to the literature.[7] [f]Not determined. [g]Literature value.[16]

Among all the investigated samples, both **P1** and **P2** exhibited the higher photooxidation efficiencies, and their performances were better than that of the conventional triplet photosensitizer MB. Here, **P3**, though containing a fullerene moiety, showed a lower efficiency, and **P4** with only a PDI moiety did not exhibit a noticeable spectral response to the light exposure. Thus, in this case, we attributed the enhanced photosensitizing ability of **P1** and **P2** to the synergetic effect of C_{60} and PDI: the PDI unit had a strong absorption of visible light, then the energy transfer from the excited singlet PDI to C_{60} occurred and resulted in the S_1 excited state of C_{60}, and the highly efficient ISC of C_{60} would eventually lead to a population of the triplet C_{60}.[1,5] From the photosensitivity data, it could be found that the double C_{60} moieties in **P2** gave a higher photooxidation efficiency compared to that of **P1** with a single C_{60}. The photooxidation rate constant of **P2** increased 1.3-fold compared to that of **P1** and increased 1.4-fold compared to that of MB. This had been identified by the results of the nanosecond time-resolved transient absorption spectroscopy in Figure 6, where **P1** had one C_{60} to store the energy from the singlet PDI. **P2** should have higher triplet C_{60} yield due to its double C_{60} moieties; thus, the spectral intensity of **P2** at various delay times were higher than that of **P1** at the corresponding time points. However, although **P2** contained two C_{60} moieties, we failed to observe a 2-fold enhancement of the spectral intensity in **P2** in comparison to that in **P1**. The reason for this difference is in the low excitation intensity of the laser, which could not pump the PDI moiety at high frequency and, in turn, populated all attached C_{60} to the triplet state. The quantitative relationship between the input intensity and fluorescence or the triplet moiety yield goes beyond the scope of this work and remains a subject of future investigation.

■ CONCLUSIONS

In summary, two axially symmetrical rigid visible light-harvesting PDI-fullerene systems, dyad **P1** with only one C_{60} and triad **P2** with two C_{60} units, have been designed and synthesized. These two molecules show high solubility in common solvents and are axially symmetrical with a rigid biphenyl as linker, ensuring a relatively constant spatial distance between the donor and acceptor and thus a unique photo-

DOI: 10.1021/acs.joc.6b02042
J. Org. Chem. 2016, 81, 12223−12231

physical property. Steady-state and time-resolved transient studies, electrochemistry, as well as TD-DFT calculations have been used to analyze the photophysical procedures of the two systems. The results indicate that the excited state is dominated by an intramolecular energy transfer from the perylene antenna to the C_{60} acceptor. The high intersystem crossing efficiency of C_{60}, which leads to a high triplet yield accompanied by the excellent absorption of PDI in the visible region, makes the dyad and triad ideal photosensitizers. This property has been substantiated by the photooxidation experiment, where both **P1** and **P2** give photooxidation efficiencies better than that of the conventional triplet photosensitizer MB and significantly higher than those of the references **P3** and **P4**, indicating a synergetic effect of C_{60} and PDI. Consistent with the results of the nanosecond time-resolved transient absorption spectroscopy, an even better performance for **P2** has been observed with its photooxidation rate constant increasing 1.3-fold compared to that of **P1** and 1.4-fold relative to MB. The combination of light-harvesting unit and intersystem crossing unit results in a highly efficient photooxidation system, which can be employed as a general structural motif for a heavy-atom-free organic triplet photosensitizer.

EXPERIMENTAL SECTION

General Methods. An absorption spectrometer and a fluorescence spectrophotometer were used to record the room-temperature UV−vis absorption and fluorescence spectra, respectively. The fluorescence lifetime measurements were performed at room temperature using a time-correlated single photon counting (TCSPC) apparatus, and a pulsed laser at a wavelength of 450 nm was applied as the excitation source. The nanosecond transient absorption spectra were performed on a nanosecond flash photolysis system. A pulse laser (7 ns, 10 Hz) from a Nd:YAG at a wavelength of 532 nm was used as the pump source. All samples in 10 mm path length quartz cells were deoxygenated by bubbling nitrogen over 20 min before measurement. The decay curves were fitted with least-squares regression using a custom-written algorithm in Matlab. All electrochemical measurements were performed under a nitrogen atmosphere at room temperature using an electrochemical analyzer. Cyclic voltammetry was performed in a three-electrode cell equipped with a platinum disc working electrode, a platinum wire counter electrode, and a calomel electrode as the standard electrode. Quantum calculations were performed with the Gaussian 09 package. The molecular structure optimization and excited-state property calculations were performed at the CAM-B3LYP/3-21G level.

*Synthesis of N-tert-Butoxycarbonyl Benzidine (**2**).* 4,4′-Diaminobiphenyl **1** (1.54 g, 8.4 mmol) was dissolved in 1,4-dioxane (30 mL). After stirring at room temperature under argon atmosphere for 30 min, a solution of Boc_2O (1.83 g, 8.4 mmol) in 1,4-dioxane (10 mL) was added dropwise over 30 min. The reaction mixture was allowed to stir at room temperature for 24 h under an argon atmosphere. Then, the solvent was removed by rotary evaporator; the residue was redissolved in dichloromethane, and then silica gel was added to absorb the mixture. After pumping off the volatiles, the resulting residue was separated on silica gel using petroleum ether-AcOEt (4:1) as the eluent to afford *N-tert*-butoxycarbonyl benzidine (**2**)[37] as a faint yellow powder (2.02 g, 85%). ^{1}H NMR (400 MHz, $CDCl_3$) δ 7.45 (d, J = 8.6 Hz, 2H), 7.36 (d, J = 8.5 Hz, 4H), 6.73 (d, J = 8.5 Hz, 2H), 6.52 (bs, 1H), 3.69 (bs, 2H), 1.52 (s, 9H).

*Synthesis of Ethyl 2-((4′-((tert-Butoxycarbonyl)amino)-[1,1′-biphenyl]-4-yl)amino)acetate (**3**).* Compound **2** (0.75 g, 2.6 mmol) was dissolved in DMF (1.5 mL) in a 25 mL single-necked round-bottomed flask. After the mixture was stirred at room temperature under an argon atmosphere for 30 min, anhydrous K_2CO_3 (0.62 g, 4.5 mmol) was added, and the mixture was allowed to stir under argon for another 10 min. Then, $BrCH_2CO_2Et$ (295 μL, 2.7 mmol) was added quickly, and argon was maintained for another 10 min before the flask was equipped with an airproof stopper. The reaction mixture was stirred at room temperature for 12 h, and the solvent was removed under reduced pressure. Then, the residue was redissolved in dichloromethane, and silica gel was added before dichloromethane was removed. The resulting solid residue was separated on silica gel using petroleum ether/AcOEt (4:1) as the eluent to produce ethyl 2-((4′-((*tert*-butoxycarbonyl)amino)-[1,1′-biphenyl]-4-yl)amino)acetate (**3**) as a faint yellow powder (0.66 g, 68%). ^{1}H NMR (400 MHz, $CDCl_3$) δ 7.45 (d, J = 8.7 Hz, 2H), 7.41 (d, J = 8.7 Hz, 2H), 7.37 (d, J = 8.6 Hz, 2H), 6.67 (d, J = 8.6 Hz, 2H), 6.49 (bs, 1H), 4.26 (q, J = 7.1 Hz, 2H), 3.93 (s, 2H), 1.53 (s, 9H), 1.30 (t, J = 7.1 Hz, 3H); ^{13}C NMR (100 MHz, $CDCl_3$; all 1C unless indicated) δ 171.2, 153.0, 146.3, 136.9, 136.2, 130.9, 127.8 (2C), 126.9 (2C), 119.1 (2C), 113.5 (2C), 80.7, 61.5, 46.1, 28.5 (3C), 14.4; HRMS (MALDI-TOF) m/z calcd for $C_{21}H_{26}N_2O_4$ $[M]^+$ 370.1893, found 370.1880.

*Synthesis of Compound **P3**.* The solution of **3** (162.4 mg, 0.44 mmol), C_{60} (152.4 mg, 0.21 mmol), and ethyl glyoxylate (225 μL, 1.14 mmol) in ODCB (8 mL) was bubbled with argon for 1 h at room temperature and then heated to 150 °C for 4 h with stirring. After the solvent was removed under reduced pressure, the mixture was subjected to column chromatography on silica gel (1:1 CS_2/CH_2Cl_2) to give **P3** as a brown powder (86.9 mg, 35%) and unreacted C_{60} (80.8 mg, 53%). ^{1}H NMR (400 MHz, $CS_2/CDCl_3$) δ 7.62 (d, J = 8.5 Hz, 2H), 7.55 (d, J = 8.5 Hz, 2H), 7.43 (d, J = 8.4 Hz, 2H), 7.33 (d, J = 8.6 Hz, 2H), 6.53 (s, 2H), 6.51 (bs, 1H), 4.31−4.18 (m, 4H), 1.54 (s, 9H), 1.17 (t, J = 7.1 Hz, 6H); ^{13}C NMR (100 MHz, $CS_2/CDCl_3$ with $Cr(acac)_3$ as relaxation reagent; all 2C unless indicated) δ 169.58, 153.01, 152.13 (1C), 150.13, 147.20, 146.16, 146.11, 145.84 (4C), 145.50, 145.41 (4C), 145.35, 145.33, 145.07, 145.01, 144.28, 144.22, 144.03 (1C), 142.85, 142.50, 142.42, 141.96, 141.89, 141.67, 141.65, 141.53, 141.47, 139.93, 139.36, 137.16 (1C), 136.59, 135.91, 134.88 (1C), 134.32 (1C), 127.41, 126.98, 118.99, 118.69, 80.03 (1C), 74.05, 70.75, 61.61, 28.13 (3C), 14.03; FT-IR ν/cm^{-1} (KBr) 2973, 2926, 1733, 1702, 1612, 1505, 1367, 1161, 823, 579, 527; UV−vis ($CHCl_3$) λ_{max}/nm 275, 308, 428, 693; HRMS (MALDI-TOF) m/z calcd for $C_{85}H_{30}N_2O_6$ $[M]^+$ 1174.2104, found 1174.2100.

*Synthesis of Compound **4**.* A solution of **P3** (100.9 mg, 0.09 mmol) and TFA (2.0 mL) in $CHCl_3$ (12 mL) was stirred under argon for 2 h at room temperature. After the solvent was removed, the mixture was separated by column chromatography on silica gel with $CHCl_3$ as the eluent, affording **4** as a brown powder (87.6 mg, 95%). ^{1}H NMR (300 MHz, $CS_2/CDCl_3$) δ 7.57 (d, J = 8.6 Hz, 2H), 7.41 (d, J = 8.4 Hz, 2H), 7.30 (d, J = 8.6 Hz, 2H), 6.73 (d, J = 8.4 Hz, 2H), 6.52 (s, 2H), 4.31−4.15 (m, 4H), 3.69 (s, 2H), 1.17 (t, J = 7.1 Hz, 6H); ^{13}C NMR (75 MHz, $CS_2/CDCl_3$; all 2C unless indicated) δ 169.95, 153.39, 150.54, 147.53, 146.49, 146.44, 146.16 (4C), 145.83, 145.77 (4C), 145.67 (3C), 145.57, 145.40, 145.33, 144.61, 144.56, 143.71 (1C), 143.18, 142.82, 142.74, 142.29, 142.22, 142.00 (4C), 141.86, 141.81, 140.25, 139.69, 136.95, 136.26, 135.33 (1C), 130.93 (1C), 127.70, 127.29, 119.35, 115.49, 74.41, 71.11, 61.84, 14.31; FT-IR ν/cm^{-1} (KBr) 3446, 3421, 2923, 2026, 1732, 1636, 1620, 1501, 1385, 1271, 1180, 1137, 873; UV−vis ($CHCl_3$) λ_{max}/nm 274, 310, 428, 690; HRMS (MALDI-TOF) m/z calcd for $C_{80}H_{22}N_2O_4$ $[M]^+$ 1074.1580, found 1074.1578.

*Synthesis of Compounds **P1** and **P4**.* A mixture of **4** (61.0 mg, 0.06 mmol), 5,6,12,13-tetrakis(4-(*tert*-butyl)phenoxy)anthra[2,1,9-def:6,5,10-d′e′f′]diisochromene-1,3,8,10-tetraone (**5**) (55.3 mg, 0.06 mmol), and imidazole (84.3 mg, 1.24 mmol) was stirred under argon atmosphere at 80 °C in $CHCl_3$ (15 mL) for 3 days (monitored by TLC). Then, aniline (20 μL, 0.22 mmol) was added, and the reaction mixture was allowed to react at 80 °C for 24 h. The mixture was cooled to room temperature and washed with water. The aqueous phase was extracted with $CHCl_3$, and the combined organic phase was dried over anhydrous Na_2SO_4. After the solvent was removed, the residue was purified by column chromatography on silica gel with toluene as the eluent to give **P4** as a red solid (24.2 mg, 38%) and **P1** as a dark red solid (42.9 mg, 36%). **P4**: ^{1}H NMR (300 MHz, $CDCl_3$) δ 8.24 (s, 4H), 7.53−7.41 (m, 6H), 7.26−7.21 (m, 12H), 6.85 (d, J = 8.7 Hz, 8H), 1.26 (s, 36H); ^{13}C NMR (75 MHz, $CDCl_3$) δ 163.6, 156.2, 152.9, 147.5, 135.3, 133.2, 129.4, 128.8, 128.6, 126.8, 122.6,

DOI: 10.1021/acs.joc.6b02042
J. Org. Chem. 2016, 81, 12223−12231

120.8, 120.2, 119.9, 119.5, 34.5, 31.5; UV−vis ($CHCl_3$) λ_{max}/nm 456, 504, 544, 586; FT-IR ν/cm^{-1} (KBr) 2961, 1706, 1673, 1588, 1504, 1407, 1340, 1315, 1288, 1206, 1175, 839. HRMS (ESI-TOF) m/z calcd for $C_{76}H_{66}N_2NaO_8$ $[M]^+$ 1157.4717, found 1157.4678. **P1**: ^{1}H NMR (400 MHz, $CDCl_3$) δ 8.29 (s, 2H), 8.25 (s, 2H), 7.77 (d, J = 8.3 Hz, 2H), 7.72 (d, J = 8.5 Hz, 2H), 7.53−7.43 (m, 3H), 7.39 (d, J = 8.6 Hz, 2H), 7.35 (d, J = 8.3 Hz, 2H), 7.26−7.22 (m, 10H), 6.87 (d, J = 8.6 Hz, 4H), 6.86 (d, J = 8.6 Hz, 4H), 6.57 (s, 2H), 4.34−4.20 (m, 4H), 1.274 (s, 18H), 1.270 (s, 18H), 1.17 (t, J = 7.1 Hz, 6H); ^{13}C NMR (100 MHz, $CDCl_3$ with $Cr(acac)_3$ as relaxation reagent) δ 170.10, 163.65, 163.54, 156.14, 156.09, 153.28, 152.86, 152.81, 150.42, 147.47, 147.41, 147.39, 146.41, 146.34, 146.09, 145.70, 145.68, 145.64, 145.61, 145.57, 145.32, 145.26, 145.01, 144.50, 144.46, 143.05, 142.73, 142.65, 142.19, 142.14, 141.90, 141.86, 141.78, 141.75, 140.97, 140.15, 139.61, 136.83, 136.14, 135.18, 134.16, 133.99, 133.18, 133.16, 129.27, 128.88, 128.69, 128.51, 128.25, 127.60, 126.66, 122.64, 122.59, 120.85, 120.75, 120.28, 120.16, 119.88, 119.80, 119.37, 119.33, 119.16, 74.40, 71.08, 61.96, 34.34, 31.42, 14.19; FT-IR ν/cm^{-1} (KBr) 2961, 1708, 1672, 1622, 1591, 1503, 1439, 1204, 1174, 963, 879, 831, 720, 580, 551, 529; UV−vis ($CHCl_3$) λ_{max}/nm 274, 292, 456, 504, 544, 586; HRMS (MALDI-TOF) m/z calcd for $C_{150}H_{81}N_3O_{12}$ $[M]^+$ 2116.5854, found 2116.5893.

Synthesis of Compound ***P2***. A mixture of **4** (59.6 mg, 0.06 mmol), 5,6,12,13-tetrakis(4-(*tert*-butyl)phenoxy)anthra[2,1,9-def:6,5,10-d′e′f′]diisochromene-1,3,8,10-tetraone (**5**) (21.6 mg, 0.02 mmol), and imidazole (153.0 mg, 2.25 mmol) was stirred under an argon atmosphere at 90 °C in $CHCl_3$ (10 mL) for 5 days (monitored by TLC). Then, the mixture was cooled and washed with water. The aqueous phase was extracted with $CHCl_3$, and the combined organic phase was dried over anhydrous Na_2SO_4. After the solvent was removed, the residue was purified with column chromatography using toluene as the eluent to provide **P2** as a dark red solid (29.7 mg, 44%). ^{1}H NMR (400 MHz, $CDCl_3$) δ 8.29 (s, 4H), 7.77 (d, J = 8.4 Hz, 4H), 7.72 (d, J = 8.5 Hz, 4H), 7.38 (d, J = 8.5 Hz, 4H), 7.35 (d, J = 8.4 Hz, 4H), 7.25 (d, J = 8.8 Hz, 8H), 6.87 (d, J = 8.8 Hz, 8H), 6.57 (s, 4H), 4.33−4.20 (m, 8H), 1.28 (s, 36H), 1.16 (t, J = 7.1 Hz, 12H); ^{13}C NMR (100 MHz, $CDCl_3$ with $Cr(acac)_3$ as relaxation reagent) δ 169.74, 163.28, 155.76, 152.93, 152.50, 150.07, 147.13, 147.03, 146.06, 145.99, 145.75, 145.32, 145.29, 145.27, 145.22, 144.98, 144.92, 144.66, 144.16, 144.12, 142.70, 142.39, 142.31, 141.85, 141.79, 141.55, 141.51, 141.43, 141.40, 140.61, 139.80, 139.26, 136.47, 135.78, 133.79, 133.63, 132.84, 128.55, 127.92, 127.27, 126.32, 122.29, 120.50, 119.92, 119.53, 119.00, 118.82, 74.04, 70.71, 61.66, 33.99, 31.09, 13.88; UV−vis ($CHCl_3$) λ_{max}/nm 274, 292, 456, 504, 544, 586; FT-IR ν/cm^{-1} (KBr) 2958, 1707, 1674, 1588, 1503, 1405, 1340, 1285, 1178, 1015, 880, 838, 819, 578, 553, 527. HRMS (MALDI-TOF) m/z calcd for $C_{224}H_{96}N_4O_{16}$ $[M]^+$ 3098.6888, found 3098.6865.

Photooxidation Details. The photooxidation experiments were carried out by following similar methods to those reported by the Zhao group.[3] DHN (1.0×10^{-4} mol L^{-1}) and triplet photosensitizer (1.0×10^{-5} mol L^{-1}) were dissolved in a mixture of CH_2Cl_2/MeOH (9:1, v/v) in a two neck round-bottom flask (25 mL), and O_2 was bubbled through the solution for 10 min. The solution was then irradiated using a 70 W xenon lamp with 0.72 M $NaNO_2$ aqueous solution as a cutoff filter. UV−vis absorption spectra were recorded at intervals of approximately 5 min. The consumption of DHN was monitored by the decrease of the UV absorption at 301 nm, and the production of juglone was recorded by an increase in the absorption at 427 nm. The photostability experiments for **P1** and **P2** were carried out with the same procedure except without DHN.

■ ASSOCIATED CONTENT

Supporting Information

The Supporting Information is available free of charge on the ACS Publications website at DOI: 10.1021/acs.joc.6b02042.

UV−vis absorption and fluorescence spectra of **P1**−**P4** in the solid state, emission of **P1**, **P2**, and **P4** in different solvents, time-resolved fluorescence spectroscopy of **P4**, calculation details, nanosecond time-resolved transient absorption spectroscopy of **P3** and the mixture of **P3** and **P4**, photooxidation details, stability of **P1** and **P2** with continuous illumination for 1 h, and NMR spectra of synthesized compounds (PDF)

■ AUTHOR INFORMATION

Corresponding Authors

*E-mail: gwang@ustc.edu.cn.

*E-mail: wangxf@iccas.ac.cn.

Notes

The authors declare no competing financial interest.

■ ACKNOWLEDGMENTS

The authors are grateful for financial support from the National Natural Science Foundation of China (21132007) and Specialized Research Fund for the Doctoral Program of Higher Education (20123402130011). We would like to thank Prof. Qun Zhang and Mr. Qi-Chao Shang for the help in the measurements of the steady-state UV−vis absorption and fluorescence spectra and time-resolved fluorescence spectra.

■ REFERENCES

(1) Guldi, D. M.; Hungerbühler, H.; Asmus, K.-D. *J. Phys. Chem.* **1995**, *99*, 9380.

(2) Sommer, T.; Kruse, T.; Roth, P. *J. Phys. B: At., Mol. Opt. Phys.* **1996**, *29*, 4955.

(3) Liu, Y.; Zhao, J. *Chem. Commun.* **2012**, *48*, 3751.

(4) Stackow, R.; Schick, G.; Jarrosson, T.; Rubin, Y.; Foote, C. S. *J. Phys. Chem. B* **2000**, *104*, 7914.

(5) Dimitrijević, N. M.; Kamat, P. V. *J. Phys. Chem.* **1993**, *97*, 7623.

(6) Schuster, D. I.; Cheng, P.; Jarowski, P. D.; Guldi, D. M.; Luo, C.; Echegoyen, L.; Pyo, S.; Holzwarth, A. R.; Braslavsky, S. E.; Williams, R. M.; Klihm, G. *J. Am. Chem. Soc.* **2004**, *126*, 7257.

(7) Arbogast, J. W.; Darmanyan, A. P.; Foote, C. S.; Rubin, Y.; Diederich, F. N.; Alvarez, M. M.; Anz, S. J.; Whetten, R. L. *J. Phys. Chem.* **1991**, *95*, 11.

(8) Baffreau, J.; Perrin, L.; Leroy-Lhez, S.; Hudhomme, P. *Tetrahedron Lett.* **2005**, *46*, 4599.

(9) Huang, D.; Zhao, J.; Wu, W.; Yi, X.; Yang, P.; Ma, J. *Asian J. Org. Chem.* **2012**, *1*, 264.

(10) Wu, Y.; Li, Y.; Li, H.; Shi, Q.; Fu, H.; Yao, J. *Chem. Commun.* **2009**, 6955.

(11) Hofmann, C. C.; Lindner, S. M.; Ruppert, M.; Hirsch, A.; Haque, S. A.; Thelakkat, M.; Köhler, J. *Phys. Chem. Chem. Phys.* **2010**, *12*, 14485.

(12) Hahn, U.; Nierengarten, J.-F.; Delavaux-Nicot, B.; Monti, F.; Chiorboli, C.; Armaroli, N. *New J. Chem.* **2011**, *35*, 2234.

(13) Yang, P.; Wu, W.; Zhao, J.; Huang, D.; Yi, X. *J. Mater. Chem.* **2012**, *22*, 20273.

(14) Wu, W.; Zhao, J.; Sun, J.; Guo, S. *J. Org. Chem.* **2012**, *77*, 5305.

(15) Baffreau, J.; Ordronneau, L.; Leroy-Lhez, S.; Hudhomme, P. *J. Org. Chem.* **2008**, *73*, 6142.

(16) Huang, L.; Yu, X.; Wu, W.; Zhao, J. *Org. Lett.* **2012**, *14*, 2594.

(17) Vail, S. A.; Schuster, D. I.; Guldi, D. M.; Isosomppi, M.; Tkachenko, N.; Lemmetyinen, H.; Palkar, A.; Echegoyen, L.; Chen, X.; Zhang, J. Z. H. *J. Phys. Chem. B* **2006**, *110*, 14155.

(18) Schuster, D. I.; Li, K.; Guldi, D. M.; Palkar, A.; Echegoyen, L.; Stanisky, C.; Cross, R. J.; Niemi, M.; Tkachenko, N. V.; Lemmetyinen, H. *J. Am. Chem. Soc.* **2007**, *129*, 15973.

(19) Apperloo, J. J.; Martineau, C.; van Hal, P. A.; Roncali, J.; Janssen, R. A. J. *J. Phys. Chem. A* **2002**, *106*, 21.

(20) Koeppe, R.; Sariciftci, N. S. *Photochem. Photobiol. Sci.* **2006**, *5*, 1122.

(21) Iglesias, R. S.; Claessens, C. G.; Torres, T.; Aminur Rahman, G. M.; Guldi, D. M. *Chem. Commun.* **2005**, 2113.

DOI: 10.1021/acs.joc.6b02042
J. Org. Chem. 2016, 81, 12223−12231

(22) Martini, I. B.; Ma, B.; Da Ros, T.; Helgeson, R.; Wudl, F.; Schwartz, B. J. *Chem. Phys. Lett.* **2000**, *327*, 253.
(23) Martín, N. *Chem. Commun.* **2006**, 2093.
(24) Huang, L.; Cui, X.; Therrien, B.; Zhao, J. *Chem. - Eur. J.* **2013**, *19*, 17472.
(25) Jones, B. A.; Ahrens, M. J.; Yoon, M.-H.; Facchetti, A.; Marks, T. J.; Wasielewski, M. R. *Angew. Chem.* **2004**, *116*, 6523.
(26) Würthner, F. *Chem. Commun.* **2004**, 1564.
(27) Le Pleux, L.; Smeigh, A. L.; Gibson, E.; Pellegrin, Y.; Blart, E.; Boschloo, G.; Hagfeldt, A.; Hammarström, L.; Odobel, F. *Energy Environ. Sci.* **2011**, *4*, 2075.
(28) Wang, N.; Li, Y.; He, X.; Gan, H.; Li, Y.; Huang, C.; Xu, X.; Xiao, J.; Wang, S.; Liu, H.; Zhu, D. *Tetrahedron* **2006**, *62*, 1216.
(29) Gómez, R.; Segura, J. L.; Martín, N. *Org. Lett.* **2005**, *7*, 717.
(30) Odom, S. A.; Kelley, R. F.; Ohira, S.; Ensley, T. R.; Huang, C.; Padilha, L. A.; Webster, S.; Coropceanu, V.; Barlow, S.; Hagan, D. J.; Van Stryland, E. W.; Brédas, J.-L.; Anderson, H. L.; Wasielewski, M. R.; Marder, S. R. *J. Phys. Chem. A* **2009**, *113*, 10826.
(31) Huang, C.; Sartin, M. M.; Siegel, N.; Cozzuol, M.; Zhang, Y.; Hales, J. M.; Barlow, S.; Perry, J. W.; Marder, S. R. *J. Mater. Chem.* **2011**, *21*, 16119.
(32) Hofmann, C. C.; Lindner, S. M.; Ruppert, M.; Hirsch, A.; Haque, S. A.; Thelakkat, M.; Köhler, J. *J. Phys. Chem. B* **2010**, *114*, 9148.
(33) Hua, J.; Meng, F.; Ding, F.; Li, F.; Tian, H. *J. Mater. Chem.* **2004**, *14*, 1849.
(34) Baffreau, J.; Leroy-Lhez, S.; Vân Anh, N.; Williams, R. M.; Hudhomme, P. *Chem. - Eur. J.* **2008**, *14*, 4974.
(35) Sukegawa, J.; Schubert, C.; Zhu, X.; Tsuji, H.; Guldi, D. M.; Nakamura, E. *Nat. Chem.* **2014**, *6*, 899.
(36) Konev, A. S.; Khlebnikov, A. F.; Nikiforova, T. G.; Virtsev, A. A.; Frauendorf, H. *J. Org. Chem.* **2013**, *78*, 2542.
(37) Fischer-Durand, N.; Rejeb, S. B.; Le Goffic, F. *Synth. Commun.* **1998**, *28*, 963.
(38) Langhals, H.; Jona, W. *Angew. Chem., Int. Ed.* **1998**, *37*, 952.
(39) Hua, J.; Meng, F.; Ding, F.; Tian, H. *Chem. Lett.* **2004**, *33*, 432.
(40) Baffreau, J.; Leroy-Lhez, S.; Hudhomme, P.; Groeneveld, M. M.; van Stokkum, I. H. M.; Williams, R. M. *J. Phys. Chem. A* **2006**, *110*, 13123.
(41) Shibano, Y.; Umeyama, T.; Matano, Y.; Tkachenko, N. V.; Lemmetyinen, H.; Araki, Y.; Ito, O.; Imahori, H. *J. Phys. Chem. C* **2007**, *111*, 6133.
(42) Chamberlain, T. W.; Davies, E. S.; Khlobystov, A. N.; Champness, N. R. *Chem. - Eur. J.* **2011**, *17*, 3759.
(43) Shibano, Y.; Umeyama, T.; Matano, Y.; Tkachenko, N. V.; Lemmetyinen, H.; Imahori, H. *Org. Lett.* **2006**, *8*, 4425.
(44) Ma, B.; Sun, Y.-P. *J. Chem. Soc., Perkin Trans. 2* **1996**, 2157.
(45) Kitamura, N.; Sakuda, E. *J. Phys. Chem. A* **2005**, *109*, 7429.
(46) Wang, X.-F.; Zhang, X.-R.; Wu, Y.-S.; Zhang, J.-P.; Ai, X.-C.; Wang, Y.; Sun, M.-T. *Chem. Phys. Lett.* **2007**, *436*, 280.
(47) Martín, N.; Sánchez, L.; Illescas, B.; Pérez, I. *Chem. Rev.* **1998**, *98*, 2527.
(48) Nierengarten, J.-F. *Sol. Energy Mater. Sol. Cells* **2004**, *83*, 187.
(49) Segura, J. L.; Martín, N.; Guldi, D. M. *Chem. Soc. Rev.* **2005**, *34*, 31.
(50) Hudhomme, P. *C. R. Chim.* **2006**, *9*, 881.
(51) Persson, N.-K.; Sun, M.; Kjellberg, P.; Pullerits, T.; Inganäs, O. *J. Chem. Phys.* **2005**, *123*, 204718.
(52) Sun, M. *J. Chem. Phys.* **2006**, *124*, 054903.
(53) Takizawa, S. Y.; Aboshi, R.; Murata, S. *Photochem. Photobiol. Sci.* **2011**, *10*, 895.
(54) Guo, S.; Wu, W.; Guo, H.; Zhao, J. *J. Org. Chem.* **2012**, *77*, 3933.
(55) Ormond, A. B.; Freeman, H. S. *Dyes Pigm.* **2013**, *96*, 440.

DOI: 10.1021/acs.joc.6b02042
J. Org. Chem. 2016, 81, 12223−12231